The Order−Disorder Transition and the Disordered Micelle Regime for Poly(ethylenepropylene-*b*-dimethylsiloxane) Spheres

Xiaohui Wang,[†,§] Elena E. Dormidontova,[‡,⊥] and Timothy P. Lodge*[,†,‡]

Department of Chemistry and Department of Chemical Engineering & Materials Science, University of Minnesota, Minneapolis, Minnesota 55455-0431

Received June 26, 2002

ABSTRACT: Two asymmetric poly(ethylenepropylene-*b*-dimethylsiloxane) diblock copolymer melts have been examined by rheology, small-angle X-ray scattering (SAXS), and small-angle neutron scattering (SANS). The two copolymers have total molecular weights of 24 400 and 23 900 and PDMS volume fractions of 0.12 and 0.10, respectively. The latter copolymer was obtained by extensive fractionation of the former, the difference in composition arising primarily from the removal of traces of PDMS homopolymer. The order−disorder transition (ODT) is unambiguously identified by rheology and SAXS. Above the ODT the SANS and rheological properties are consistent with the recently proposed disordered micelle regime, whereby the copolymers are associated in micellar aggregates that are not ordered on a lattice. The viscosity of the melt in this regime is greater than that of a poly(ethylenepropylene) homopolymer of the same total molecular weight. The SANS structure factors were analyzed by a generalized inverse Fourier transform and by direct fitting to a model based on the Percus−Yevick structure factor and either a spherical or an ellipsoidal form factor. Both approaches give comparable results, and the average micelle core radius, effective hard-sphere radius, and volume fraction were extracted as a function of temperature. The fitting suggests that as temperature increases the micelles remain relatively unchanged, but their number density and volume fraction decrease steadily. The fractionated copolymer has a significantly smaller micellar core than its precursor and therefore a significantly smaller aggregation number. These differences are attributable to the partitioning of PDMS homopolymer into the micellar cores. For these samples the critical micelle temperature (cmt), where the volume fraction of micelles should become negligible, was not accessed, even 100 deg above the ODT.

Introduction

Because of the chemical bond linking the different components, block copolymers tend to exhibit "microphase separation" instead of macroscopic phase separation. This self-association phenomenon endows block copolymers with appealing physical and mechanical properties that have received considerable attention.[1−4] A great deal is known about the factors that dictate the selection of a particular morphology within the ordered state, and self-consistent mean-field (SCMF) theory in particular is often capable of near-quantitative calculations of ordered state free energies and structural details. However, in the vicinity of the order−disorder transition (ODT) and in the disordered state away from the ODT, such quantitative success is still lacking. Furthermore, there remain significant unresolved issues even at the qualitative level. Several of these concern highly asymmetric copolymers, which adopt the bcc packing of spherical micelles in the ordered state. In this paper we present a detailed experimental examination of two such copolymers at and above the ODT, in an attempt to clarify aspects of the behavior in this regime.

In Leibler's pioneering mean-field theory,[5] the equilibrium state of a diblock copolymer in the weak segregation limit is determined by only two parameters. These are the volume fraction of the minor block (f) and the product χN, where χ ($\sim 1/T$) is the Flory−Huggins parameter characterizing the enthalpic interactions between the different segments and N is the total number of segments in the chain. For asymmetric diblock melts, Leibler predicted a direct first-order phase transition to a body-centered-cubic (bcc) phase from the disordered melt on increasing χN. The disordered state was treated via the random phase approximation (RPA), i.e., as a random mixture of Gaussian chains. Fredrickson and Helfand presented the first attempt to incorporate the effect of composition fluctuations near the ODT[6] and were able to capture at least qualitatively many of the experimental deviations from the Leibler theory.[7] However, this treatment becomes quantitatively less reliable as either N or f decreases. Schweizer and co-workers used the PRISM model to study the equilibrium properties of the disordered state.[8−10] Although for symmetric copolymer melts they obtained similar results to the Fredrickson−Helfand theory, the microscopic origin of the fluctuations was found to be enthalpic rather than entropic in nature; furthermore, the differences between the two approaches increase as f decreases. However, as a liquid state theory the PRISM model cannot find the ODT directly.

Part of the difficulty with asymmetric copolymers arises because as f decreases the expected value of $(\chi N)_{ODT}$ increases, from ca. 10 when $f = 0.5$ to ca. 50 when $f \approx 0.1$. Consequently, the degree of segregation is rather strong even in the disordered state, and treatments based on perturbations about a Gaussian reference state may encounter difficulties. Semenov recognized this feature and considered the ODT for

† Department of Chemistry.
‡ Department of Chemical Engineering & Materials Science.
§ Current address: Polymer Division, National Institute of Standards and Technology, Gaithersburg, MD 20899.
⊥ Current address: Department of Macromolecular Science and Engineering, Case Western Reserve University, Cleveland, OH 44106-7202.
* Author for correspondence: e-mail lodge@chem.umn.edu.

10.1021/ma021009j CCC: $22.00
Published on Web 11/19/2002

asymmetric copolymers in terms of the relative stability of various packings of preexisting spherical micelles.[11,12] Under certain conditions phase sequences such as disordered → face-centered cubic (fcc) → hexagonally close-packed (hcp) → bcc upon cooling were anticipated. Detailed SCMF calculations by Matsen and Bates reached a similar conclusion, namely that there was a narrow window of a stable close-packed structure (i.e., fcc or hcp) between bcc and disorder.[13] As far as we are aware, such a close-packed sphere phase has yet to be reported for a diblock copolymer melt. Recently, we extended Semenov's approach to consider the possible stability of a disordered micelle regime above the ODT and found that such a state can indeed intervene in place of a close-packed structure.[14]

Experimentally, three groups have studied the ODT from bcc spheres and the neighboring disordered phase in some detail, utilizing poly(styrene-*b*-isoprene) (SI) diblock and triblock copolymers. Schwab and Stühn employed small-angle X-ray scattering (SAXS) to examine the temperature dependence of $S(q)$ for a polymer with $f = 0.11$.[15,16] They reported a stable state of liquidlike micelles between the microscopically homogeneous, fully disordered state at high temperature and the bcc ordered array of spheres at low temperature. They analyzed the scattering profiles quantitatively in the framework of the Percus−Yevick theory for hard-sphere liquids[17] and found that both the micellar core size and the hard-sphere radius decrease with increasing temperature, through a decrease in the mean aggregation number of the micelles. The number density of micelles remained roughly constant, however. The volume fraction (ϕ_{hs}) of hard spheres was about 0.47 at the ordering transition, which compares favorably to the value $\phi_{hs} = 0.494$ where a hard-sphere liquid adopts the fcc packing.[18]

Register and co-workers have emphasized the location of the ODT itself for SI copolymers, as determined by SAXS and rheology.[19,20] In the latter case, the low-frequency dynamic elastic modulus G' exhibited a sharp drop at the ODT, in a manner qualitatively similar to lamellar, cylinder, or gyroid-forming copolymers. Below T_{ODT} they found a metastable liquidlike arrangement of polystyrene spheres, which is kinetically trapped by a combination of the high viscosity as the T_g of PS is approached and the relatively small thermodynamic driving force to form the bcc lattice. For some samples this structure developed into a bcc phase after sufficient annealing. Above the T_{ODT}, they attributed the deviation of the scattering profiles from Leibler's mean-field theory to large-amplitude composition fluctuations, in analogy with more symmetric copolymers. They further suggested that the liquidlike spherical state may simply result from the vitrification of large-amplitude composition fluctuations.

More recently, Han, Hashimoto, and Kim and co-workers have examined similar systems by SAXS, rheology, and TEM.[21−24] Han et al. identify two transitions, termed the lattice disordering/ordering transition (LDOT) and the demicellization/micellization transition (DMT).[21] The LDOT is defined as a transition where the long-range order of spheres is lost during heating, giving rise to a disordered arrangement of spheres with short-range liquidlike order; it thus corresponds to the ODT of the other groups. The DMT is defined as a transition where all the spheres disappear during heating, leading to a micelle-free state in which the block copolymers are fully mixed on a molecular level. The experimental signatures of the DMT are much more subtle than those of the LDOT/ODT, and in fact it is not even clear whether a distinct transition exists. For example, Dormidontova and Lodge conclude that there is no phase transition where micelles disappear but that rather the micelle number fraction decreases continuously with increasing temperature.[14] Thus, the disordered micelle regime and the fully disordered state belong to one disordered phase.

Following conventional terminology, we define the ODT as the transition where long-range order disappears and the critical micelle temperature (cmt) as the highest temperature where distinct micelles can be discerned experimentally. Thus, our ODT and cmt should correspond to the LDOT and DMT of Han et al., respectively.[21] The main objectives of this work are (1) to confirm whether liquidlike micelles exist as a thermodynamic equilibrium state above T_{ODT}, as predicted by recent theory[14] and as reported by previous workers,[15,16,21−24] (2) to characterize the temperature dependence of the liquid structure in this regime in more detail, and (3) to assess whether there is a clear transition (cmt) from a liquidlike micelle regime to a micelle-free, "fully" disordered state. As a model system, SI is far from ideal: it is hampered by a limited accessible temperature range, bounded below by the high PS T_g (ca. 100 °C) and above by the thermal instability of PI ($T \geq 200$ °C). In addition to this limited thermodynamic window, the strongly temperature-dependent and sluggish PS chain dynamics often contribute to severe kinetic limitations. In contrast, both poly(ethylenepropylene) (PEP) and poly(dimethylsiloxane) (PDMS) have low T_g (<−70 °C), and the thermal stability of PEP is far superior to the unsaturated PI precursor. Consequently, PEP−PDMS copolymers offer a wider accessible temperature window, with relatively rapid chain dynamics. In this paper we report the determination of the ODT via rheology and SAXS, and a detailed examination of the liquidlike micelle regime above T_{ODT}, via rheology and small-angle neutron scattering (SANS), for two PEP−PDMS diblocks with $f_{PDMS} = 0.12$ and 0.10.

Experimental Section

Synthesis and Characterization. Poly(ethylenepropylene-*b*-dimethylsiloxane) (ED) was prepared by anionic polymerization of a precursor polymer, poly(isoprene-*b*-dimethylsiloxane) (ID), followed by hydrogenation/deuteration of the polyisoprene (PI) block. Isoprene was polymerized in cyclohexane at 45 °C using *sec*-butyllithium as initiator. After 4 h, ca. 5 mL of living PI solution was taken out through a cannula, terminated with 2-propanol, and dried without further purification to provide a PI precursor for characterization. At room temperature we added hexamethylcyclotrisiloxane (D_3) into the cyclohexane solution of living PI chains, resulting in the termination of the isoprene polymerization by the addition of three methylsiloxane units. The solution was then stirred overnight to allow for complete reaction, before 250 mL of THF was added to start propagation at room temperature. Because of PDMS redistribution reactions (which, however, are slow compared to the propagation reaction), the polymerization was terminated by 3-(trimethylsiloxypropyl)-dimethylchlorosilane after 1 h, before complete conversion of D_3 was achieved. After most of the solvent was removed in a rotovap, 50 mL of cyclohexane was added, and the reaction solution was washed with distilled water six times to remove salt. Finally, ID was precipitated in a mixture of methanol and 2-propanol (volume 1:1) and completely dried in a vacuum oven. ID was completely (>99.5%) hydrogenated or deuterated

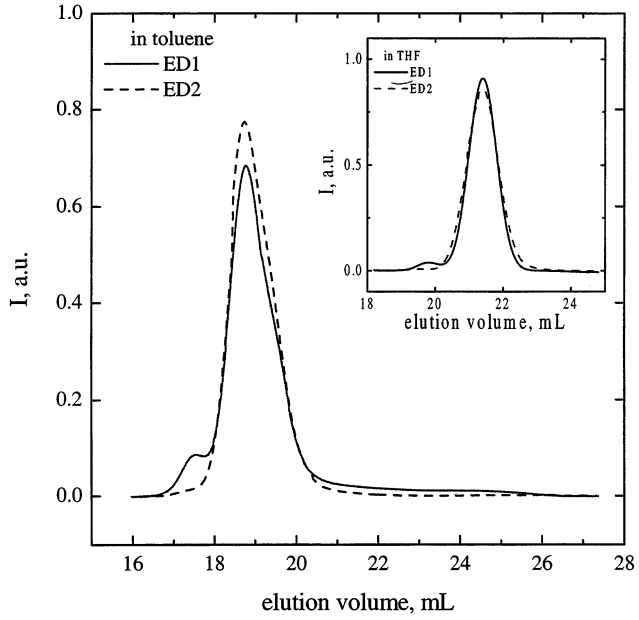

Figure 1. SEC traces for unfractionated (ED-1) and fractionated (ED-2) samples.

at 35 atm and 60 °C using palladium (5%) on calcium carbonate as catalyst in cyclohexane, following standard procedures.[25]

Nuclear magnetic resonance (NMR) was used to determine the PI precursor molecular weight and microstructure, to determine the ID and ED copolymer composition, and to check the extent of hydrogenation of ED. Size exclusion permeation chromatography (SEC) was used to characterize the polydispersity of the samples and the molecular weight of the PI precursor using PI standards. The inset to Figure 1 shows the SEC trace for ED in THF and indicates a narrowly distributed polymer with a small bump corresponding to the coupled triblock. This sample was subjected to SANS, SAXS, and rheology measurements. However, certain aspects of the results motivated recharacterization. An SEC trace for the same polymer in toluene in Figure 1 reveals the presence of a small amount of broadly distributed PDMS homopolymer, which was not observed before due to the near refractive index match between THF and PDMS. Accordingly, ED was fractionated in a chloroform/methanol system at 2−5% w/v concentration four times, to remove small amounts of triblock and PDMS homopolymer. The SEC trace in toluene for the fractionated sample is also shown in Figure 1, and it is evident that most of the contaminants are removed. The characterization results are summarized in Table 1, and the samples before and after fractionation are designated ED-1 and ED-2, respectively. NMR showed the PI microstructure to be ca. 95% 1,4- and 5% 3,4-, and therefore ED contains some 2-propylethylene segments in the PEP block after hydrogenation. The PI molecular weight from NMR is slightly smaller than that from SEC, due presumably to the low intensity of the initiator peak. We take $20._7 \times 10^3$ g/mol as the PI molecular weight, and thus the PEP block in ED has $M = 21._3 \times 10^3$ g/mol. From the ID copolymer molar composition the PDMS block in ED-1 has $M = 3.1 \times 10^3$ g/mol, and the volume fraction $f = 0.120$ at 25 °C is estimated via the temperature dependence of the density of PEP and PDMS:[26]

$$\rho_{PEP} = 1.054 \exp(-6.977 \times 10^{-4} T) \quad (g/mL) \qquad (1)$$

$$\rho_{DMS} = 1.195 \exp(-6.998 \times 10^{-4} T) \quad (g/mL) \qquad (2)$$

From the copolymer molar composition the PDMS block in ED-2 has $M = 2.6 \times 10^3$ g/mol and volume fraction $f = 0.098$ at 25 °C.

Rheology. An Advanced Rheometric Expansion System (ARES) was used with parallel plate fixtures (50 mm diameter) and a ca. 1 mm gap. Three different types of experiment in the oscillatory mode and one in the steady mode were conducted. (1) Dynamic temperature ramp experiments: dynamic storage and loss moduli (G' and G'') were measured under isochronal conditions at a fixed heating rate of 0.3 or 0.5 °C/min. (2) Dynamic strain sweep experiments: G' and G'' were measured as a function of strain amplitude (γ) ranging from 0.1% to 100% to determine the linear viscoelastic regime at fixed angular frequency (ω) and different temperatures. (3) Dynamic frequency sweep experiments: G' and G'' were measured as a function of ω ranging from 0.01 to 100 rad/s at various fixed temperatures during a heating cycle. (4) Steady rate sweep experiments: the viscosity (η) was measured as a function of shear rate ranging from 1 to 100 s^{-1}. This measurement was used to obtain the zero-shear viscosity when the dynamic frequency sweep failed to provide reliable data (below ca. 200 Pa·s). ED-1 and ED-2 samples were annealed for 6 h at 185 and 160 °C, respectively, in an attempt to obtain reasonably well-ordered bcc structures, and each specimen was kept at a constant temperature for 30 min before the measurements were begun. The temperature control was accurate to within ±1 °C, and all measurements were taken under a nitrogen atmosphere. After the high-temperature rheology tests the samples were checked by SEC for sample degradation; no measurable degradation was found for samples that did not exceed 300 °C.

Table 1. Polymer Characterization

	NMR			SEC	
polymer	M_n (10^3 g/mol)	x^a	f	M_n (10^3 g/mol)	M_w/M_n
PI	$19._0$			$20._7$	1.03
ID		0.12_8			1.05
ED-1			0.12_0		1.05
ED-2		0.11_0	0.09_8		1.04

[a] x is the mole fraction of the PDMS block in ID.

Small-Angle X-ray Scattering (SAXS). SAXS measurements were performed at the University of Minnesota using a Rigaku RU-200BVH rotating anode X-ray generator producing Cu Kα radiation ($\lambda = 1.542$ Å). The instrument makes use of focusing optics (Franks mirrors) and an area detector (Siemens). The sample-to-detector distance was 2.25 m, and the sample was held in an O-ring (thickness ca. 1 mm) between two Kapton windows. Temperature was controlled to within ±1 °C. Intervals for thermal equilibrium and exposure for each scan were 10 and 15 min, respectively. The resulting two-dimensional images were averaged azimuthally to obtain a trace of intensity vs the scattering wave vector q ($q = 4\pi \sin(\theta/2)/\lambda$, where θ is the scattering angle).

Small-Angle Neutron Scattering (SANS). SANS measurements were performed on the NIST/Exxon/University of Minnesota 30 m instrument (NG7) at the National Institute of Standards and Technology, Gaithersburg, MD, using a wavelength of $\lambda = 6.0$ Å with $\Delta\lambda/\lambda = 0.11$ and sample-to-detector distance of 7 m. Samples were loaded between quartz disks separated by a 1.1 mm aluminum spacer and then sealed with high-temperature adhesive. Partially deuterated d-ED-1 and d-ED-2 samples were annealed prior to the measurements, at 180 ± 10 °C for 6 h and at 160 ± 1 °C for 5 days, respectively. Temperature was controlled to within ±1 °C in the SANS heating stage. Raw data were corrected for detector sensitivity and beam-blocked instrumental background detector counts and then normalized for sample transmission and sample thickness. Absolute calibration was accomplished using a Sil A5 standard. The two-dimensional scattering images were averaged azimuthally to produce one-dimensional absolute scattering intensity as a function of the scattering wave vector q. The incoherent scattering intensity for pure d-PEP and PDMS was used to estimate the incoherent scattering intensity of d-ED.

Results

The results are organized as follows. First we locate the ODT by rheology and SAXS and then describe the

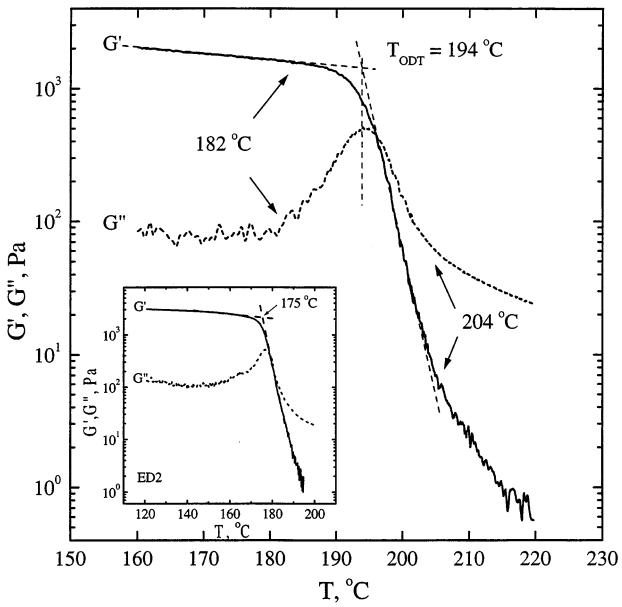

Figure 2. Temperature dependence of the dynamic storage and loss moduli (G' and G'') for ED-1 upon heating from 160 to 220 °C at 0.3 °C/min, with $\omega = 1$ rad/s and $\gamma = 2.0\%$. The inset shows the temperature dependence of the dynamic storage and loss moduli (G' and G'') for ED-2 upon heating from 120 to 195 °C at 0.5 °C/min, with $\omega = 1$ rad/s and $\gamma = 1.0\%$.

SANS results in the disordered micelle regime in some detail. In some cases data are presented for both ED-1 and ED-2, as the comparison affords useful insight into which features of the copolymer response are influenced by added homopolymer. To anticipate the main conclusion in this regard, the qualitative features of the response are unaffected, but the quantitative details of the micellar structure in the disordered regime are significantly altered.

The Order−Disorder Transition. The power of rheology, and the low-frequency elastic modulus in particular, to locate phase transitions in block copolymers is well documented.[4,27] Figure 2 shows the temperature dependence of G' and G'' of ED-1 when the sample was heated from 160 to 220 °C at 0.3 °C/min, with $\omega = 1$ rad/s and $\gamma = 2.0\%$. The main feature is the rapid 2 orders of magnitude drop in G' that begins near 194 °C and is accompanied by maximum in G''. This rheological signature of the ODT is clearest when the sample has been annealed for a sufficiently long time in the ordered state to produce a well-defined bcc lattice. At ca. 182 °C, G' first starts to decrease rapidly and G'' starts to increase during heating; this may be identified as the first "softening" of the lattice. Above ca. 204 °C, the rate of decrease of G' and G'' with increasing temperature decreases rather abruptly; the possible significance of this feature will be discussed subsequently. The inset of Figure 2 shows the temperature dependence of G' and G'' of ED-2 when the sample was heated from 120 to 195 °C at 0.5 °C/min, with $\omega = 1$ rad/s and $\gamma = 1.0\%$. The ED-2 profile is similar to ED-1, but the ODT moves to lower temperature ($T_{ODT} = 175$ °C); this change in ODT is not due to the slightly increased heating rate.

To determine the limit of linear viscoelastic response within these different temperature regions, we carried out dynamic strain sweep experiments on ED-1 at 170, 190, 198, and 210 °C. For all these temperatures, the higher the frequency, the greater the strain amplitude that remained within the linear regime. At 170 °C, the apparent low-frequency strain limit is 5%, consistent with the reported small deformability of the bcc structure;[28] in fact, it is quite possible that the true limit of linear response is even smaller but extremely hard to detect.[29] As temperature increases, the width of the linear viscoelastic regime increases continuously. At 210 °C, both G' and G'' are independent of strain amplitude up to 100%, which is suggestive of a disordered state.

Using time−temperature superposition (TTS), G' and G'' of ED-1 at different temperatures were compared as a function of the reduced angular frequency (ωa_T) as shown in parts a and b of Figure 3, respectively. The shift factor (a_T) was determined from the temperature dependence of the viscosity of a poly(ethylenepropylene) (PEP) homopolymer with a molecular weight of 2.4×10^4 g/mol using the following Williams−Landel−Ferry (WLF) equation:[30,31]

$$\log a_T = \frac{-5.50(T - 25)}{139 + (T - 25)} \tag{3}$$

It is apparent from Figure 3 that TTS does not work very well, as expected for a material passing through a phase transition, but the format shows clearly that there are three regimes of behavior, especially in G'. Below 170 °C, there is a plateau in G' extending over 4 decades in reduced frequency; this behavior is symptomatic of a cubic phase.[29] Above 215 °C the profiles become parallel to one another with $G' \sim \omega^2$ and $G'' \sim \omega$, indicating terminal or liquidlike behavior. It is worth noting that there is a large drop in amplitude for both moduli between 195 and 200 °C, which is just above the ODT as determined in Figure 2. For the intermediate regime, between 170 and 215 °C, the amplitude of G' decreases and the apparent plateau narrows. It is also instructive to plot G' vs G'', as shown in Figure 3c. In this format three regimes are also clearly evident, with the same boundaries as in Figure 3a,b: there is a low-frequency plateau below 170 °C, an intermediate regime up to ca. 215 °C, and then terminal behavior with complete superposition of the traces for different temperatures. The dynamic frequency sweep experiments on ED-2 at different temperatures gave similar features and so are not shown here.

Figure 4 shows the SAXS profiles of ED-1 at various temperatures ranging from 161 to 225 °C during a heating cycle. At 161 °C, there is a primary peak with two clear higher-order peaks at $q = \sqrt{2}q^*$ and $q = \sqrt{3}q^*$, where q^* is the primary peak position, indicating a well-developed bcc structure. (Strictly these data are not sufficient to rule out simple cubic packing, but based on extensive experimental and theoretical precedent, bcc is almost certainly the actual symmetry.) From 161 to 193 °C, the sharpness and intensity of the primary peak decrease, while the higher-order peaks become gradually harder to discern. Near 195 °C the primary peak broadens distinctly, and the higher-order peaks disappear; thus, the long-range order of the bcc structure has melted at the ODT. From 195 to 204 °C, the primary peak still can be resolved although it continues to broaden. By 225 °C the relatively weak signal and the high-temperature limit on the SAXS instrument prevented further measurement; however, this important regime can be explored by SANS as discussed below.

To quantify the evolution of the primary peak with increasing temperature, a Lorentzian fit was used over

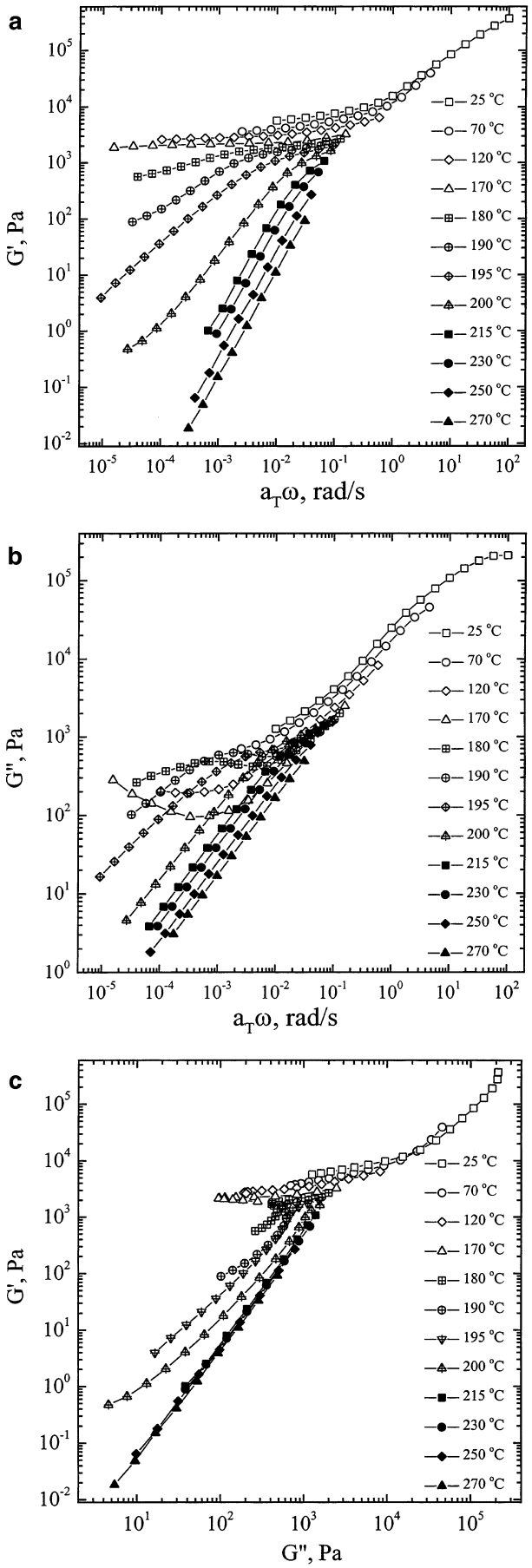

Figure 3. For ED-1, (a) G' vs reduced frequency using shift factors from pure PEP, at the indicated temperatures; (b) G'' plotted as in (a); (c) G' vs G'' from the data in (a) and (b).

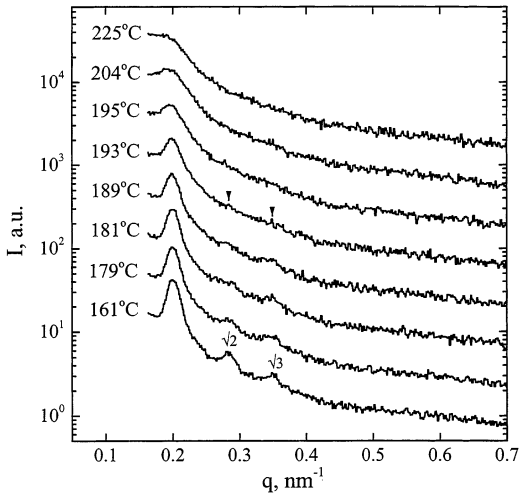

Figure 4. For ED-1, temperature dependence of the SAXS profiles (intensity vs q) after heating to the indicated temperatures. Each trace has been shifted up by $^1/_3$ decade relative to the next lower temperature.

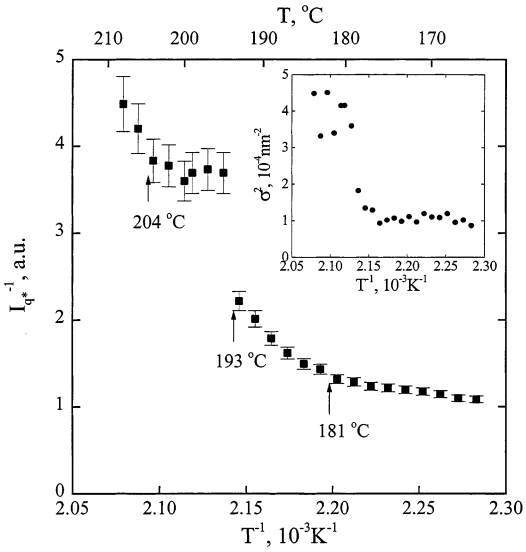

Figure 5. For ED-1, inverse primary SAXS peak intensity vs inverse temperature; the ODT is clearly defined. The inset shows the squared peak half-width at half-maximum, which also increases abruptly at the ODT. Other temperatures are indicated for comparison with the moduli in Figure 2.

a narrow interval around the maximum and above the background to obtain the primary peak position, q^*, intensity, $I(q^*)$, and half-width at half-maximum (σ). The reciprocal of $I(q^*)$ is plotted vs the reciprocal of the absolute temperature (T^{-1}) in Figure 5, and the square of σ is shown in the inset. As temperature increases, $I(q^*)$ decreases while σ^2 increases. Both $1/I(q^*)$ and σ^2 show an abrupt increase between 193 and 195 °C, indicating that the ODT is a first-order phase transition; furthermore, the location of the ODT coincides with that from rheology. The rate of increase of $1/I(q^*)$ with temperature in the ordered state starts to increase perceptibly near 181 °C, where G' and G'' showed the first indication of the approaching ODT (Figure 2). From 195 to 204 °C, $1/I(q^*)$ does not change very much; because of the proximity of the beam stop (see Figure 4) and the decreasing intensity, it is difficult to determine $I(q^*)$ and σ^2 above 204 °C precisely. ED-2 gave similar SAXS features near its T_{ODT}.

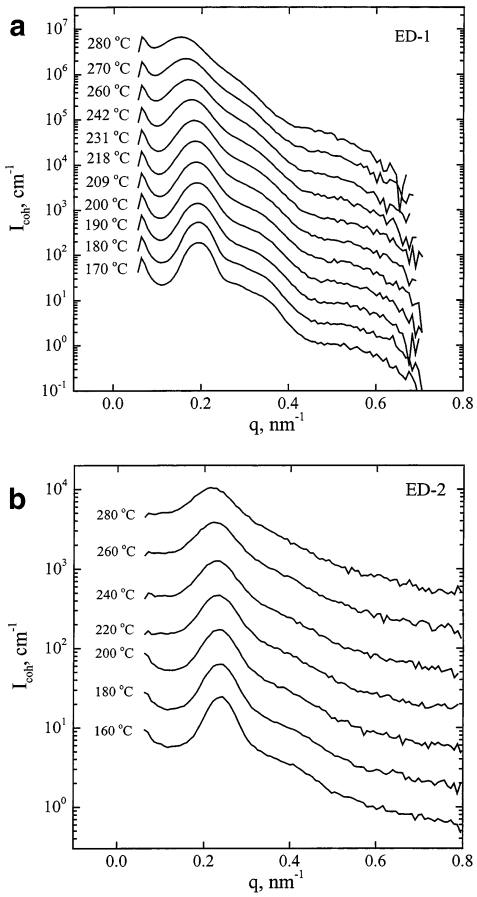

Figure 6. Temperature dependence of the SANS profiles (intensity vs q) after heating to the indicated temperatures. Each trace has been shifted up by $^1/_3$ decade relative to the next lower temperature. (a) ED-1 and (b) ED-2.

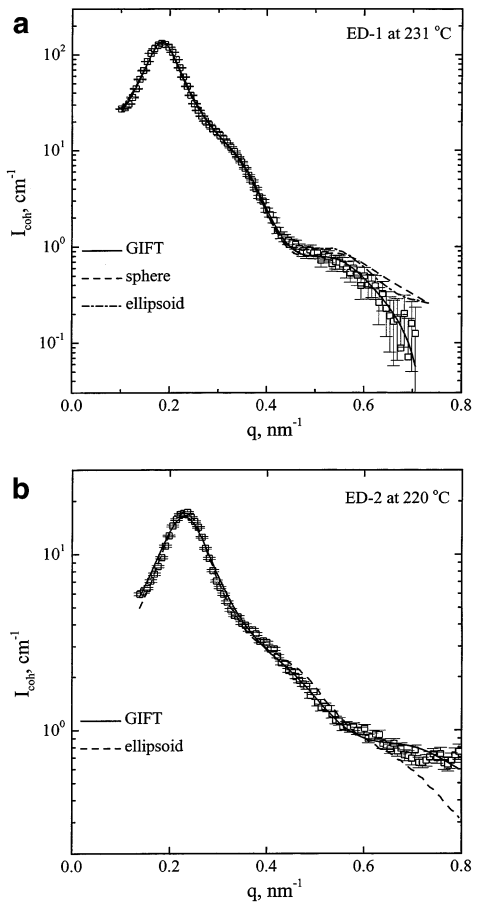

Figure 7. SANS traces (a) ED-1 at 231 °C and (b) ED-2 at 220 °C, compared to fits from the generalized inverse Fourier transform (GIFT) and the Percus−Yevick effective hard-sphere model with spherical and ellipsoidal form factors.

Disordered Micelle Regime. Parts a and b of Figure 6 show the temperature dependence of SANS profiles during a heating cycle at various temperatures up to 280 °C for ED-1 and ED-2, respectively. The data are shifted vertically for each temperature for clarity. The features of scattering profiles for both samples are similar, but the primary peak positions (q^*) are clearly different. Because of the lower resolution in SANS compared with SAXS, the primary peak is not particularly sharp, and the higher-order peaks are not well resolved in the profiles below T_{ODT}. However, there is a very clear shoulder on the high q side of the primary peak for both samples. Most importantly, this shoulder persists well above T_{ODT}, even up to the 280 °C limit of the experiment. This feature confirms a nonrandom arrangement of chains, that following the previous workers[15,16,21−23] we will interpret as micelles. In contrast, the mean-field theory of Leibler anticipates a single broad peak due to the correlation hole effect and cannot describe these data.[5] It seems reasonable to take approximate adherence to the Leibler structure factor as a necessary condition for having passed through the cmt; on this basis our results indicate that the disordered micelle regime persists to at least 100 °C above the ODT for these samples.

The coherent neutron scattering intensity of a spherical micelle system can be written

$$I \propto P(q)\, S(q) \tag{4}$$

where $P(q)$ is the form factor, accounting for the intraparticle correlations, and $S(q)$ is the structure factor, accounting for the interparticle correlations. We now employ two independent approaches to analyzing the SANS data: an indirect Fourier transform and a direct model fitting. Both approaches have limitations, especially for data that are relatively limited in q range and intensity, but in this case they provide consistent results. First, we use the Global Indirect Fourier Transformation (GIFT) software developed by Glatter and co-workers to fit the scattering profiles.[32] In GIFT, there is no model or analytical restriction for $P(q)$, but $S(q)$ is parametrized with up to four parameters for a given interaction model. We find that the Percus−Yevick (PY)[17] apparent average hard-sphere model, combined with an unconstrained form factor for a polydisperse system, fits the data very well over the entire q range and at all temperatures above the ODT for both samples. Parts a and b of Figure 7 give two examples of the fitting, for ED-1 at 231 °C and ED-2 at 220 °C, respectively. From these fits we extract the number-average micelle core radius, R_c, from $P(q)$ through the micelle core size distribution $D(R_c)$, and an effective hard-sphere radius, R_{hs}, and volume fraction of effective hard spheres, ϕ_{hs}, from $S(q)$. The results are listed in Tables 2 and 3 for ED-1 and ED-2, respectively. The main features of these parameters for both samples are similar. The average micelle core radius remains constant at first, before increasing slightly for ED-1 or decreasing slightly for ED-2 with increasing temperature above 240 °C, and the volume fraction of micelles

Table 2. Summary of GIFT Fitting Parameters for ED-1

T, °C	R_c, nm	R_{hs}, nm	$R_{hs} - R_c$, nm	ϕ_{hs}
199	11.0	16.8	5.8	0.376
209	11.0	16.8	5.8	0.367
218	11.0	16.8	5.8	0.358
231	11.0	17.0	6.0	0.347
241	11.0	16.6	5.6	0.328
260	11.6	17.3	5.7	0.288
270	12.0	17.6	5.6	0.262
280	12.5	18.0	5.5	0.223

Table 3. Summary of GIFT Fitting Parameters for ED-2

T, °C	R_c, nm	R_{hs}, nm	$R_{hs} - R_c$, nm	ϕ_{hs}
180	8.1	13.3	5.2	0.328
200	8.1	13.2	5.1	0.307
220	8.1	13.0	4.9	0.275
240	7.8	13.1	5.3	0.266
260	7.8	13.0	5.2	0.233
280	7.8	13.3	5.5	0.213

for both samples decreases steadily throughout this temperature range. There is no clear evidence of any distinct transition above the ODT, such as a cmt.

Figure 8 shows typical GIFT structure factors $S(q)$ for ED-1 at different temperatures. The oscillations become progressively less pronounced with the increasing temperature, indicating that the higher the temperature, the lower the intermicellar correlations, but the presence and liquidlike arrangement of micelles are indicated across this temperature range. As shown in the inset, q^* remains nearly constant below 240 °C and then shifts to lower q values, implying that the mean distance between micelles does not change much below 240 °C and then increases with temperature. (Note that the exact value of q^* may not be simply related to any physical length in the system, during the evolution from a lattice of spheres to a melt of chains.) Figure 9 shows typical size distribution functions $D(R_c)$ at various temperatures for ED-1. Because the shape of $D(R_c)$ can be sensitive to the upper bound on R_c (R_{max}), R_{max} was varied to obtain the best fit; Figure 9 shows the results where R_{max} is around 16 nm for all temperatures. There are small oscillations for $R_c < 7$ nm that probably arise from the noise in the data at high q and the instrumental smearing. In summary, the GIFT analysis shows that the scattering intensity can be well described by a spherical form factor $P(q)$ combined with an $S(q)$ in the PY hard-sphere approximation.

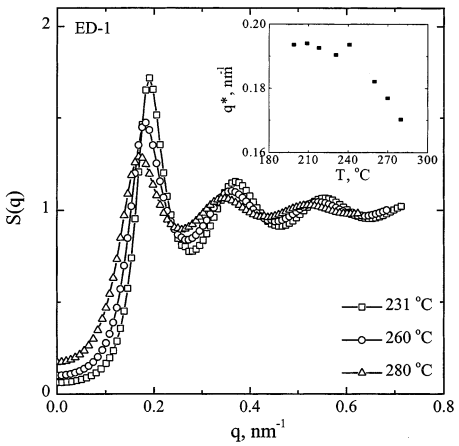

Figure 8. Representative structure factors $S(q)$ from the generalized inverse Fourier transform at the indicated temperatures for ED-1. The inset shows the position of the scattering maximum.

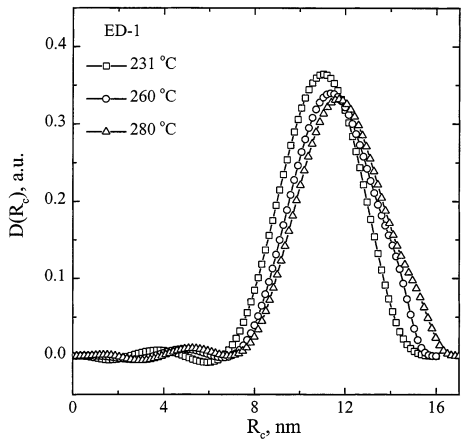

Figure 9. Representative size distribution functions $D(R_c)$ for the micellar core radius at the indicated temperatures for ED-1.

We now use the PY model to fit the ED-1 scattering profiles directly, taking into account core size polydispersity, interfacial thickness, and instrumental smearing effects, in hope of extracting a more detailed picture of the micelles above T_{ODT}. This approach is very similar to that employed by Kinning and Thomas[33] (who fitted experimental data of Berney et al.[34]) and Schwab and Stühn.[15,16] For monodisperse solid spheres $P(q)$ can be represented by

$$P(q,R) = \left[\frac{3(\sin(qR) - qR\cos(qR))}{(qR)^3}\right]^2 \qquad (5)$$

where R is the radius of the sphere. For the micellar melt we take $R = R_c$, where R_c is the radius of the micellar core formed by the PDMS block and PDMS homopolymer; in other words, the system is viewed as a suspension of PDMS spheres in a homogeneous matrix comprising the corona chains plus free diblock copolymer chains. Polydispersity in the micellar core radius is accounted for by convoluting the spherical form factor with a distribution function. Previously, a Gaussian distribution with a standard deviation of σ_c has been used, and to account for the details at higher q, a diffuse sphere boundary parameter ξ was introduced.[33] In this way $P(q)$ becomes

$$P(q,R_c,\sigma_c,\xi) = \frac{\exp(-4\pi^2\xi^2q^2)}{\sigma_c\sqrt{2\pi}}\int_0^\infty \exp\left(\frac{-(R-R_c)^2}{2\sigma_c^2}\right)P(q,R)\,dR \qquad (6)$$

where $P(q,R)$ is given by eq 5.

For $S(q)$ the simplest correlations to consider result from a hard-sphere potential between micelles, with disordered (liquidlike) packing of the micelles in the matrix. Ornstein and Zernike first described the direct correlation between two hard spheres,[35] which Percus and Yevick approximated by a function with an analytical solution.[17] The resulting expression, referred to as the Percus−Yevick (PY) model, is

$$S(q,R_{hs},\phi) = \frac{1}{1 + \dfrac{24\phi G(A)}{A}}$$

$$G(A) = \frac{\alpha}{A^2}(\sin A - A\cos A) + \frac{\beta}{A^3}[2A\sin A + (2 - A^2)\cos A - 2] + \frac{\gamma}{A^5}\{-A^4\cos A + 4[(3A^2 - 6)\cos A + (A^3 - 6A)\sin A + 6]\}$$

$$\alpha = \frac{(1 + 2\phi)^2}{(1 - \phi)^4}$$

$$\beta = \frac{-6\phi(1 + \phi/2)^2}{(1 - \phi)^4}$$

$$\gamma = \frac{\phi(1 + 2\phi)^2}{2(1 - \phi)^4} \quad (7)$$

where $A = 2qR_{hs}$, with R_{hs} the effective hard-sphere radius and ϕ_{hs} the effective volume fraction of spheres. This expression can be used for any spherical system in a liquid state where the interaction between particles can be represented by a hard-sphere potential. This also works well for block copolymer micelles because of the strong entropic repulsion between micelles from the corona brushes.[33]

The calculated neutron scattering intensity was smeared to fit the measured SANS intensity $I(q_0)$ by convoluting it with the instrumental resolution function, $R(q-q_0)$, as follows:[36]

$$I(q_0) = \int I(q)\, R(q-q_0)\, dq \quad (8)$$

where $R(q-q_0)$ can be approximated by another Gaussian function:

$$R(q-q_0) = \frac{1}{\sqrt{2\pi}\sigma_q}\exp\left(-\frac{1}{2}\left(\frac{q - q_0}{\sigma_q}\right)^2\right) \quad (9)$$

where the variance of the resolution σ_q is determined by the neutron wavelength spread, detector resolution, and instrumental geometry.[36] For the configuration employed here $\sigma_q^2\,(\mathrm{nm}^{-2}) = 4.19 \times 10^{-4} + 2.18 \times 10^{-1}q^2$. It should be noted that the smearing correction has a rather minor effect on the resulting parameter values, and thus the absence of a smearing correction in the GIFT analysis is not a serious limitation.

Figure 7a also provides an example of this fitting. Except for some deviations in the higher q range, the fitting works very well. We do not attribute much significance to these deviations, partly because of the weak intensity and large error bars and partly because of the inevitable uncertainty in the incoherent background subtraction. The extracted parameters are summarized in Table 4. Comparing Tables 2 and 4, the primary conclusion is that the two approaches give identical results. The effective volume fraction ϕ_{hs} of micelles decreases continuously, and R_c remains nearly constant as the temperature increases above T_{ODT}, implying that a decrease in the number of micelles is the main reason for the decrease in ϕ_{hs}. The fact that the PDMS core volume fraction ($\phi_c = (R_c/R_{hs})^3\phi_{hs}$, assuming the core is pure PDMS) is less than the PDMS block volume fraction ($f = 0.12$) suggests that some PDMS blocks are not in micelles and are mixed with the PEP matrix. This is consistent with theoretical expectation.[13,14,37] The higher the temperature, the higher the concentration of free chains in the melt. In other words, even in the one component melt micelles and free chains can coexist above T_{ODT}. (Note that this is not a violation of the phase rule, as the system remains a single disordered phase.) There is some evidence of a weak transition around 240 °C, where both the micellar core size and its polydispersity (σ_c) first start to increase, and the corona width, which is associated with $R_{hs} - R_c$, starts to decrease. Finally, it is worth noting that the diffuse sphere boundary, ξ, does not change much with the temperature. On the basis of the approach suggested by Hashimoto et al.,[38] the boundary between the core and corona is equal to $(2\pi)^{1/2}\xi$, which gives a value of 0.2 nm in this case. Compared with the core size, we can conclude that the interface is very sharp in the liquidlike micelle regime, although this value is of course too small to be taken literally. The Helfand−Tagami theory, for example, would predict an interfacial width of ca. 1.5 nm for these polymers in this temperature range.[39]

The aggregation number of the micelles can be estimated from the core size and the density of PDMS:

$$N_{agg} = \frac{4\pi R_c(T)^3\rho(T)N_A}{3M_{PDMS}} \quad (10)$$

where N_A and M_{PDMS} are Avogadro's number and the molecular weight of the PDMS block, respectively. Over the whole temperature range N_{agg} is around 800, which is larger than the typical case for block copolymer micelles (N_{agg} of order 10^2). However, this number includes some PDMS homopolymer is presumably preferentially sequestered in the core.

We now turn briefly to the analysis of the SANS data for ED-2. The GIFT results collected in Table 3 show similar behavior to ED-1, except that the core size is significantly reduced (and consequently the inferred aggregation number, about 300). Most importantly, the volume fraction of hard spheres also decreases monotonically with increasing temperature. The direct fitting of the ED-2 SANS data was not quite as successful as with ED-1, however. A more elaborate model, which allows for some ellipticity to the micelles, was able to give a satisfactory description, as shown in Figure 7b,

Table 4. Summary of Direct Fitting the Sphere Model for ED-1

T, °C	R_c, nm	R_{hs}, nm	$R_{hs} - R_c$, nm	ϕ_{hs}	ϕ_c[a]	σ_c, nm	ξ, nm	N_{agg}
199	10.7	16.6	5.9	0.363	0.097	1.72	0.08	803
209	10.7	16.7	6.0	0.355	0.093	1.70	0.07	798
218	10.7	16.7	6.0	0.348	0.092	1.74	0.08	793
231	10.9	16.8	5.9	0.338	0.092	1.94	0.09	831
241	10.7	16.5	5.8	0.324	0.088	1.85	0.12	780
260	11.4	17.3	5.9	0.290	0.083	2.29	0.14	931
270	11.9	17.5	5.6	0.262	0.082	2.53	0.12	1052
280	12.5	17.8	5.3	0.219	0.076	2.74	0.10	1210

[a] $\phi_c = (R_c/R_{hs})^3\phi_{hs}$, i.e., the volume fraction of the PDMS core.

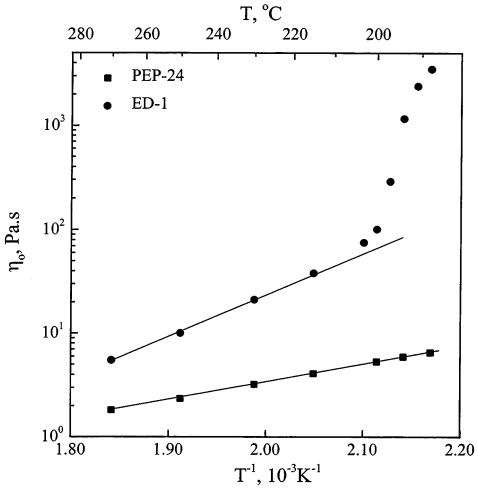

Figure 10. Reciprocal temperature dependence of the zero-shear viscosity of PEP and ED-1.

but the addition of another parameter makes us rather skeptical of the significance of this result. For example, it is not clear to what extent the various parameters such as polydispersity, interfacial width, and ellipticity are interacting in the fit. Consequently, we are inclined to place more weight on the GIFT results in this instance.

The scattering evidence for the existence of some kind of micellar aggregates in the melt above T_{ODT} is strong, but the low-frequency viscoelastic response (Figure 3) is liquidlike. If there were no micelles, the viscosity of the disordered diblock copolymer melt should be similar to that of a molecular-weight-matched homopolymer. Figure 10 shows the temperature dependence of the zero-shear viscosity for ED-1 and for a PEP homopolymer of the same total molecular weight. Over this high-temperature range the viscosity of PEP can be well described by an Arrhenius equation (which is still consistent with eq 3 at lower T). Above 204 °C η_0 of ED-1 also follows the Arrhenius equation, but with a larger activation energy. However, the copolymer viscosity is systematically higher, and from 190 to 204 °C η_0 decreases strongly as temperature increases. Even at 270 °C, η_0 of ED-1 is about 2.5 times greater than that of PEP. This result is strong evidence for some form of interchain association well above the ODT. Note that this viscosity enhancement is much too large to be attributed to the small amount of triblock, or to the PDMS homopolymer, or to the chemical difference between PDMS and PEP. In particular, PDMS has both a lower friction factor and lower entanglement density than PEP.

Discussion

Order−Disorder Transition. Our experimental results show that the ODT can be determined unambiguously by both SAXS and rheology. In SAXS the discontinuous changes in $I(q^*)^{-1}$ and σ^2 as temperature increases (Figure 5) locate T_{ODT} (194 ± 2 °C). Below the T_{ODT}, the micelles are arrayed on a bcc lattice, as higher-order peaks are clearly resolved in the scattering intensity profiles shown in Figure 4; these reflections are not evident above T_{ODT}. The rheological signatures of the ODT are also clear. A slow temperature ramp at low frequency reveals a large drop in G' at the ODT (Figure 2). Below the ODT G' shows a low-frequency plateau (Figure 3a) which is a consistent feature of cubic phases in block copolymers; this plateau disappears above the ODT. This combination of SAXS and rheological signatures of the ODT is in excellent agreement with previous reports of several groups, but others have questioned the reliability of $G'(T)$ to locate the ODT.[21,23,40] One possible cause of this difference is a poorly formed bcc lattice on the low temperature side of the ODT. It is sometimes the case that long annealing times (i.e., days) are not sufficient to form a highly organized structure, due to a combination of a small thermodynamic driving force and slow kinetics. Even in the current system, where the chain dynamics are relatively facile, several hours of annealing just below the ODT is not sufficient to guarantee a high degree of long-range order.

It should also be noted that the ODT has a finite width in these experiments. On the low temperature side the rheological properties announce the impending transition about 10 deg below T_{ODT}; this "softening" of the lattice possibly reflects the expulsion of some chains from each micelle. At and above the ODT the decrease in G' with T is not as sharp as is often seen in, for example, lamellar systems. This is attributable to the nature of the disordered state: the interactions among the congested micelles lead to a more gradual loss of dynamic elasticity. Another factor to consider is compositional heterogeneity. Although the molecular weight distribution and composition distribution of asymmetric copolymers are typically narrow and comparable to those for symmetric systems, in the asymmetric case the location of the ODT is much more sensitive to f; in other words, whereas $\partial(\chi N)_{ODT}/\partial f \approx 0$ for lamellar systems, it is much larger for $f \approx 0.1$. Consequently, the transition itself could be broadened due to phase coexistence, i.e., between a bcc phase rich in larger f or N copolymers and a disordered micelle phase rich in lower f or N molecules. Note, however, that the rheological signatures of the ODT for ED-1, which contains some triblock and some PDMS homopolymer, are comparable to those for ED-2 (see Figure 2), and therefore we conclude that polydispersity is not playing a substantial role. The small difference in T_{ODT} for the two samples is directly attributable to the small change in f upon fractionation.

The last issue to consider with respect to the ODT for highly asymmetric copolymers is whether it corresponds to the ODT for lamellar, gyroid, and cylinder-forming systems or is something distinct, as proposed for example by Han, Hashimoto, and Kim.[21−23] In particular, these authors argue that the transition considered here, which they term the LDOT or LDT, is unique to sphere-forming copolymers. We do not feel that there is a fundamental difference between the ODT for the different ordered state symmetries in block copolymers. As discussed at length elsewhere, the disordered micelle regime is part of the disordered phase and is not a separate phase.[14] Accordingly, there is only one thermodynamic phase transition between the bcc ordered state and the high temperature disordered state, the ODT, just as with cylinder and lamellae-forming copolymers. Furthermore, in all cases this transition can be consistently located by a combination of SAXS and rheology.

Disordered Micelle Regime and Micelle Parameters. The experimental results and data fitting provide a consistent picture of a liquidlike packing of micelles; the structure factors in Figure 8, especially, echo the

structure factor of a hard-sphere fluid as a function of density. This state represents a compromise between the entropic drive for complete disorder and the enthalpic drive to segregate the two monomers. On heating from the low-temperature ordered state, the balance between chains in micelles and free chains shifts in favor of free chains, eventually disrupting the bcc lattice at the ODT but without destroying all the micelles. These results are at least broadly consistent with the pioneering experimental work of Schwab and Stühn[15,16] and of Hashimoto, Han, and Kim[21−23] on the styrene−isoprene system. Furthermore, the recent calculations provide a rationale for the observation of this disordered micelle state,[14] in place of the close-packed sphere phase anticipated by self-consistent mean-field theory.[13]

Although the inversion and the direct fitting give consistent results, it is important to recognize that such analysis is often rather delicate, and it is difficult to establish that a given model is the correct one. In this case the SANS data exhibit a clear peak, a higher q shoulder, and one or two distinct dips. Whether these features are sufficient to justify the number of parameters in Table 4 is questionable. However, the SANS curves are clearly not describable by a Leibler-like structure factor, so there is evidently some nontrivial, average local structure in the fluid. Furthermore, the temperature dependence and magnitude of the viscosity are compelling evidence for the same conclusion. Consequently, although one may question the detailed values of the parameters of the fits, they do provide a plausible interpretation. Furthermore, the relative values of a given parameter, either from temperature to temperature or from ED-1 vs ED-2, are probably significant.

The parameters collected in Tables 2 and 3 (from inverse Fourier transformation) and Table 4 (from direct model fitting) provide a more detailed picture of the evolution of the structure within the liquidlike micelle regime for both ED-1 and ED-2. Beginning with Tables 2 and 3, the most important parameters are the hard-sphere volume fraction, ϕ_{hs}, and the associated hard-sphere radius, R_{hs}. These values are determined primarily by the height and location of the main peak of $S(q)$ and are therefore relatively robust. The close agreement among the hard-sphere volume fractions extracted from Tables 2 and 4 is reassuring. The trends with temperature are clear: ϕ_{hs} decreases steadily, whereas R_{hs} remains more or less constant, except above 240 °C when it apparently increases slightly. In short, the main change with temperature as one traverses the liquidlike micelle state from the ODT on up is the progressive dissolution of some micelles in favor of free chains. This is at least qualitatively consistent with the recent theory.[14] These results can be compared with that of Schwab and Stühn.[15,16] They also inferred the presence of spherical micelles, based on a detailed deconvolution of SAXS profiles. However, in contrast to our results, they found that the number of micelles remained constant but the micelle size decreased with increasing temperature. The origin of this difference is not clear.

The other important parameter to consider is the core radius, R_c. This comes from the form factor and is based on a simplified view of the structure of the fluid, namely as a suspension of PDMS spheres in a homogeneous matrix of corona blocks and free chains. Thus, the values of R_c should be viewed with some caution. For ED-1, the core size remains constant above the ODT up to about 240 °C, before increasing by a few percent. As the length of a PDMS chain in the core determines R_c, and R_c is about 3 times the unperturbed chain size ($\langle h^2 \rangle^{1/2} \approx 3.8$ nm),[26] the PDMS blocks in the core would be strongly stretched, except that the presence of PDMS homopolymer plays a role. The core sizes imply a micellar aggregation numbers of 800−900, which might be unrealistically large. However, the presence of PDMS homopolymer within the PDMS core contributes to this number significantly over the entire temperature range. The difference between R_{hs} and R_c gives the effective thickness of the "impenetrable" corona, which is constant at ca. 5.5−6 nm. This is less than the unperturbed PEP chain size, indicating that there is significant interpenetration of the corona with the surrounding matrix. For ED-2 R_c remains constant and is significantly smaller, again suggesting that solubilization of homopolymer leads to the high aggregation numbers for ED-1.

The recent calculations of the nature of the disordered micelle regime are in qualitative agreement with the trends reported here.[14] The theory anticipates a steady decrease in the volume fraction of micelles with increasing distance above the ODT, consistent with these data. However, there should be a slight decrease in the micelle core dimensions, which is not really established in these results. This theory does not take into account the presence of contaminants such as homopolymers, nor does it incorporate the possibility of micellar asymmetry or polydispersity. Finally, using estimates of the temperature dependence of χ for the PEP−PDMS system, the theory anticipates a narrower temperature window of disordered micelles than is observed experimentally. The origin of this difference remains to be resolved.

Critical Micelle Temperature. For the cmt to be a meaningful concept in this context, there should be a particular temperature (or narrow temperature range) where it occurs and which should be independently identifiable by at least two different methods. The alternative would be a smooth progression in all experimental observables from just above the ODT down to the fully disordered state. From the experiments on these two ED samples no cmt is apparent; if one exists, it must lie at higher temperatures. Consequently, we cannot resolve this interesting question at this point. However, measurements on a lower molecular weight ED sample with a lower ODT do extend into the mean-field regime; these results will be discussed in a separate publication.[41]

It is worth briefly reconsidering whether the rheological feature at 204 °C for ED-1 (see Figure 2) could correspond to the cmt. If this were the cmt, then the interval between the ODT and the cmt would be much smaller and in better agreement with the theory.[14] However, the difficulty with this interpretation is threefold. First, there is no signature of this transition in the scattering, particularly with respect to the SANS results. Second, the rheological features have a natural explanation within the context of the disordered micelle state, namely as a consequence of the sharp increase in viscosity (and longest relaxation time) on cooling as the spheres come in close proximity just prior to the ODT. Third, the SANS data remain resolutely non-mean-field to much higher temperatures; this is not consistent with the fully disordered state. Consequently,

if the cmt separates the disordered micelle regime from a fully disordered (mean-field) state, then it does not occur at 204 °C or within the temperature window of these experiments. An alternative picture would be to ascribe all of the experimental signatures to a broad fluctuation regime, in analogy to more symmetric copolymers. In particular, although the hard-sphere model is very successful in fitting the SANS structure factors, this is presumably not a unique interpretation. In this point of view there would be no experimental distinction between the fluctuation regime and the disordered micelle state. On the basis of the experimental results presented here, the scenario of a disordered micelle regime is favored, but the fluctuation description cannot be discounted.

Summary

We have examined the temperature dependence of the rheological and small-angle scattering properties of two asymmetric diblock copolymers in detail. The principal conclusions are the following:

1. The samples undergo the order−disorder transition from a bcc array of spherical micelles into a disordered state, at 194 ± 2 and 175 ± 2 °C for ED-1 and ED-2, respectively. The ODT is consistently located by the temperature dependence of G' at low frequency, by the frequency dependence of G' and G'' as a function of temperature, and by the intensity and width of the principal SAXS peak.

2. The disordered state above the ODT is consistent with the proposed "disordered micelle state", whereby some copolymer chains remain in micellar aggregates, but the micelles themselves adopt a liquidlike packing.[15,16,21−23] Detailed analysis of SANS curves suggests that as temperature increases the micelles remain relatively unchanged, but their number density and volume fraction decrease steadily. The viscosity of the fluid throughout this regime is higher than that of a corresponding homopolymer melt, which is also attributable to the presence of a significant fraction of micelles.

3. The details of the micellar characteristics are sensitive to the presence of small amounts of homopolymer, amounts that in fact are not readily discerned in routine SEC analysis. Whether such traces of homopolymer were present in previous studies is not clear, but the possibility should be considered. However, the main features of the results are not influenced greatly by such contaminants.

Acknowledgment. This work was supported by the National Science Foundation through Award DMR-9901087 and by the MRSEC Program under Award DMR-9809364. Otto Glatter was of great help with the implementation of the GIFT analysis. The assistance of Ken Hanley, Kevin Cavicchi, and Bryant Pudil with the synthesis, and Charlie Glinka, Paul Butler, and Sungmin Choi with the SANS measurements, is appreciated.

References and Notes

(1) Goodman, I. *Developments in Block Copolymers-1*; Applied Science: New York, 1982.
(2) Goodman, I. *Developments in Block Copolymers-2*; Applied Science: New York, 1985.
(3) Bates, F. S.; Fredrickson, G. H. *Annu. Rev. Phys. Chem.* **1990**, *41*, 525.
(4) Hamley, I. W. *The Physics of Block Copolymers*; Oxford University Press: Oxford, 1998.
(5) Leibler, L. *Macromolecules* **1980**, *13*, 1602.
(6) Fredrickson, G. H.; Helfand, E. *J. Chem. Phys.* **1987**, *87*, 697.
(7) Bates, F. S.; Schulz, M. F.; Khandpur, A. K.; Förster, S.; Rosedale, J. H.; Almdal, K.; Mortensen, K. *J. Chem. Soc., Faraday Discuss.* **1994**, *98*, 7.
(8) David, E. F.; Schweizer, K. S. *J. Chem. Phys.* **1994**, *100*, 7767.
(9) Guenza, M.; Schweizer, K. S. *Macromolecules* **1997**, *30*, 4205.
(10) Guenza, M.; Schweizer, K. S. *J. Chem. Phys.* **1997**, *106*, 7391.
(11) Semenov, A. N. *Sov. Phys. JETP* **1985**, *61*, 733.
(12) Semenov, A. N. *Macromolecules* **1989**, *22*, 2849.
(13) Matsen, M. W.; Bates, F. S. *J. Chem. Phys.* **1997**, *106*, 2436.
(14) Dormidontova, E. E.; Lodge, T. P. *Macromolecules* **2001**, *34*, 9143.
(15) Schwab, M.; Stühn, B. *Phys. Rev. Lett.* **1996**, *76*, 924.
(16) Schwab, M.; Stühn, B. *Colloid Polym. Sci.* **1997**, *275*, 341.
(17) Percus, J. K.; Yevick, G. *Phys. Rev.* **1958**, *28*, 6825.
(18) Hoover, W. G.; Ree, R. H. *J. Chem. Phys.* **1968**, *49*, 3609.
(19) Adams, J. L.; Graessley, W. W.; Register, R. A. *Macromolecules* **1994**, *27*, 6026.
(20) Adams, J. L.; Quiram, D. J.; Graessley, W. W.; Register, R. A.; Marchand, G. R. *Macromolecules* **1996**, *29*, 2929.
(21) Han, C. D.; Vaidya, N. Y.; Kim, D.; Shin, G.; Yamaguchi, D.; Hashimoto, T. *Macromolecules* **2000**, *33*, 3767.
(22) Kim, J. K.; Lee, H. H.; Sakurai, S.; Aida, S.; Masamoto, J.; Nomura, S.; Kitagawa, Y.; Suda, Y. *Macromolecules* **1999**, *32*, 6707.
(23) Sakamoto, N.; Hashimoto, T.; Han, C. D.; Kim, D.; Vaidya, N. Y. *Macromolecules* **1997**, *30*, 1621.
(24) Sakamoto, N.; Hashimoto, T. *Macromolecules* **1995**, *28*, 6825.
(25) Rosedale, J. H.; Bates, F. S. *J. Am. Chem. Soc.* **1988**, *110*, 3542.
(26) Fetters, L. J.; Lohse, D. J.; Richter, D.; Witten, T. A.; Zirkel, A. *Macromolecules* **1994**, *27*, 4639.
(27) Fredrickson, G. H.; Bates, F. S. *Annu. Rev. Mater. Sci.* **1996**, *26*, 503.
(28) Sebastian, J. M.; Lai, C.; Graessley, W. W.; Register, R. A. *Macromolecules* **2002**, *35*, 2707.
(29) Kossuth, M. B.; Morse, D. C.; Bates, F. S. *J. Rheol.* **1999**, *43*, 167.
(30) Ferry, J. D. *Viscoelastic Properties of Polymers*, 3rd ed.; Wiley: New York, 1980.
(31) Gotro, J. T.; Graessley, W. W. *Macromolecules* **1984**, *17*, 2767.
(32) Brunner-Popela, J.; Glatter, O. *J. Appl. Crystallogr.* **1997**, *30*, 431.
(33) Kinning, D. J.; Thomas, E. L. *Macromolecules* **1984**, *17*, 1712.
(34) Berney, C. V.; Cohen, R. E.; Bates, F. S. *Polymer* **1982**, *23*, 1222.
(35) Ornstein, L. S.; Zernicke, F. *Proc. Akad. Sci. Amsterdam* **1914**, *17*, 793.
(36) Pedersen, J. S.; Posselt, D.; Mortensen, K. *J. Appl. Crystallogr.* **1990**, *23*, 321.
(37) Matsen, M. W. *Macromolecules* **1995**, *28*, 5765.
(38) Hashimoto, T.; Fujimura, M.; Kawai, H. *Macromolecules* **1980**, *13*, 1660.
(39) Helfand, E.; Tagami, Y. *J. Chem. Phys.* **1972**, *56*, 3592.
(40) Han, C. D.; Baek, D. M.; Kim, J. K.; Ogawa, T.; Sakamoto, N.; Hashimoto, T. *Macromolecules* **1995**, *28*, 5043.
(41) Wang, X.; Lodge, T. P., manuscript in preparation.

MA021009J